Basal forebrain control of olfactory bulb interneurons

Alvaro Sanz Diez[1], Marion Najac[2] and Didier De Saint Jan[1]

[1]Institut des Neurosciences Cellulaires et Intégratives, Centre National de la Recherche Scientifique, Unité Propre de Recherche 3212, Université de Strasbourg, 67084 Strasbourg, France, [2]Department of Neurobiology, Northwestern University, Evanston, Illinois 60208.

Corresponding authors:
desaintjan@inci-cnrs.unistra.fr
Institut des Neurosciences Cellulaires et Intégratives, CNRS UPR 3212, 5 rue Blaise Pascal, 67084 Strasbourg, France

Authors contributions: ASD and DDSJ did the experiments, MN contributed essential preliminary data, DDSJ wrote the paper. All authors edited the manuscript.

Abstract

Olfactory bulb circuits transform a spatially organized olfactory sensory input into a temporal output code in mitral and tufted cells. Various GABAergic interneurons modulate this early processing. However, little is known about the GABAergic circuits that regulate the activity of olfactory bulb interneurons. We examined this question using patch-clamp recording and optogenetics in olfactory bulb slices. We found that long-range centrifugal projections from the basal forebrain provide a prominent GABAergic synaptic input on most subtypes of periglomerular (PG) cells, deep short axon cells and granule cells. We also demonstrate that basal forebrain inputs have specific properties and distinct functional impacts depending on the postsynaptic PG cell subtype. Thus, centrifugal GABAergic afferents may excite, inhibit or sequentially inhibit and excite distinct PG cells using co-transmission of acetylcholine. Together, these results reinforce the idea that basal forebrain projections have multiple, complex and so far overlooked implications on olfactory bulb processing.

Introduction

Olfactory bulb circuits transform the spatially organized sensory input carried by olfactory sensory neurons (OSNs) into a temporal code in mitral and tufted cells, the principal neurons that relay the information to cortical areas. In the olfactory bulb, inhibitory interneurons, which vastly outnumber mitral and tufted cells, form several inhibitory circuits that shape the output of principal neurons. In addition, thousands of newborn inhibitory neurons are integrated every postnatal day in the pre-existing olfactory bulb network. Inhibition thus plays fundamental roles in early olfactory bulb processing, as demonstrated by multiple evidence *in vivo* (Yokoi et al., 1995; Cang and Isaacson, 2003; Abraham et al., 2010; Fukunaga et al., 2012; Lepousez and Lledo, 2013; Fukunaga et al., 2014; Gschwend et al., 2015; Economo et al., 2016).

Olfactory bulb interneurons are diverse but three large classes dominate: granule cells, periglomerular (PG) cells and short-axon (SA) cells. Granule cells, the most abundant, form reciprocal dendrodendritic synapses with the lateral dendrites of mitral and tufted cells in the external plexiform layer. These axonless neurons mediate reciprocal inhibition (Isaacson and Strowbridge, 1998; Schoppa et al., 1998) as well as lateral inhibition between principal cells projecting in different glomeruli (Isaacson and Strowbridge, 1998). PG interneurons surround spherical neuropil called glomeruli into which OSN axons make synapses onto principal neurons. These small cells that usually project within a single glomerulus and often lack an axon are functionally, morphologically and chemically highly diverse (Kosaka and Kosaka, 2007; Panzanelli et al., 2007; Parrish-Aungst et al., 2007; Whitman and Greer, 2007; Kosaka and Kosaka, 2011). Yet, they have been classified in two broad classes. The majority, so-called type 2 PG cells, receive excitatory inputs exclusively from the apical dendrites of mitral and tufted cells and in turn generate a potent intraglomerular inhibition in mitral and tufted cells (Shao et al., 2009; Shao et al., 2012; Shao et al., 2013; Najac et al., 2015; Geramita and Urban, 2017). In contrast, type 1 PG cells receive direct excitatory inputs from OSNs and modulate glutamate release from the sensory afferents (Murphy et al., 2005; Shao et al., 2009). Finally, SA cells with soma located in the glomerular layer (superficial SA cells) or in the granule cell layer (deep or dSA cells), unlike what their name suggest, possess long ramifying axons that form broad intrabulbar and interglomerular axonal connections (Aungst et al., 2003; Eyre et al., 2008; Kosaka and Kosaka, 2008; Kiyokage et al., 2010; Burton et al.,

2017). The diverse morphological subtypes of dSA cells mediate a widespread interneuron-specific inhibition (Eyre et al., 2008; Boyd et al., 2012; Burton et al., 2017) whereas superficial SA cells inhibit external tufted cells (Liu et al., 2013; Whitesell et al., 2013).

Granule, PG and SA cells receive GABAergic synaptic inputs but only few studies have investigated their origin and functional impact. GABAergic inputs could arise from local interneuron interactions. Synaptic or spillover-mediated transmission between PG cells (Smith and Jahr, 2002; Murphy et al., 2005; Parsa et al., 2015) or between granule cells (Bardy et al., 2010) have been reported. GABAergic inputs could also arise from the diverse dSA cells that contact granule, PG and other dSA cells (Eyre et al., 2008; Burton et al., 2017). Finally, several nuclei in the subcortical basal forebrain, especially the horizontal limb of the Diagonal Band of Broca (HDB), send dense centrifugal GABAergic projections to the olfactory bulb (Zaborszky et al., 1986; Gracia-Llanes et al., 2010; Niedworok et al., 2012). The HDB fibers innervate all layers of the bulb and functional connections have been demonstrated on granule (Nunez-Parra et al., 2013) and dSA cells (Case et al., 2017). Thus, different GABAergic pathways may synapse on olfactory bulb interneurons and control their activity.

We examined the GABAergic innervation of olfactory bulb interneurons, with a specific focus on PG cells, using patch-clamp recording and optogenetics in acute slices. We demonstrate that the different subtypes of type 2 PG cells do not interact between each other. Instead, they receive robust GABA inputs from the basal forebrain, each subtype being diversely modulated by this GABAergic input. We further provide evidence for co-transmission of acetylcholine and GABA on a specific subtype of type 2 PG Cells. We also show that fibers from the basal forebrain release GABA onto granule and dSA cells as well. Long-range basal forebrain GABAergic projections thus broadly regulate olfactory bulb circuits with a previously unrecognized level of synaptic complexity.

Results

The glomerular network does not provide inhibition on type 2 PG cells

We first used the Kv3.1-EYFP transgenic mouse (Metzger et al., 2002) to investigate whether PG cells innervate each other. In this reporter mouse line, a heterogeneous population of type 2 PG cells is selectively labeled and includes, although not exclusively,

calbindin-expressing PG cells. EYFP(+) PG cells respond to a single electrical stimulation of the OSNs with a short polysynaptic barrage of excitatory postsynaptic currents (EPSCs) that efficiently drives their firing (Najac et al., 2015). If EYFP(+) PG cells make synapses onto each other, a stimulation of the OSNs should also produce inhibitory postsynaptic currents (IPSCs) in these neurons. However, OSN stimulations that evoked robust excitatory responses in EYFP(+) PG cells voltage-clamped at Vh=-75 mV, did not evoke any outward IPSC when cells were clamped around the reversal potential for EPSCs (Vh=0 mV, n=15, Figure 1A and 1B). As a control, in a subset of experiments, we simultaneously monitored the firing of a PG cell projecting into the same glomerulus (either EYFP(+), n=4, or EYFP(-), n=5). Under these conditions, OSN stimulations that did produced a discharge in the control PG cell still did not evoke any IPSC in the voltage-clamped EYFP(+) PG cell (supplementary Fig.1). Increasing the stimulation intensity by a factor of 10 also failed to evoke reliable IPSCs (n=6, supplementary Fig.1). Thus, EYFP(+) PG cells do not inhibit each other.

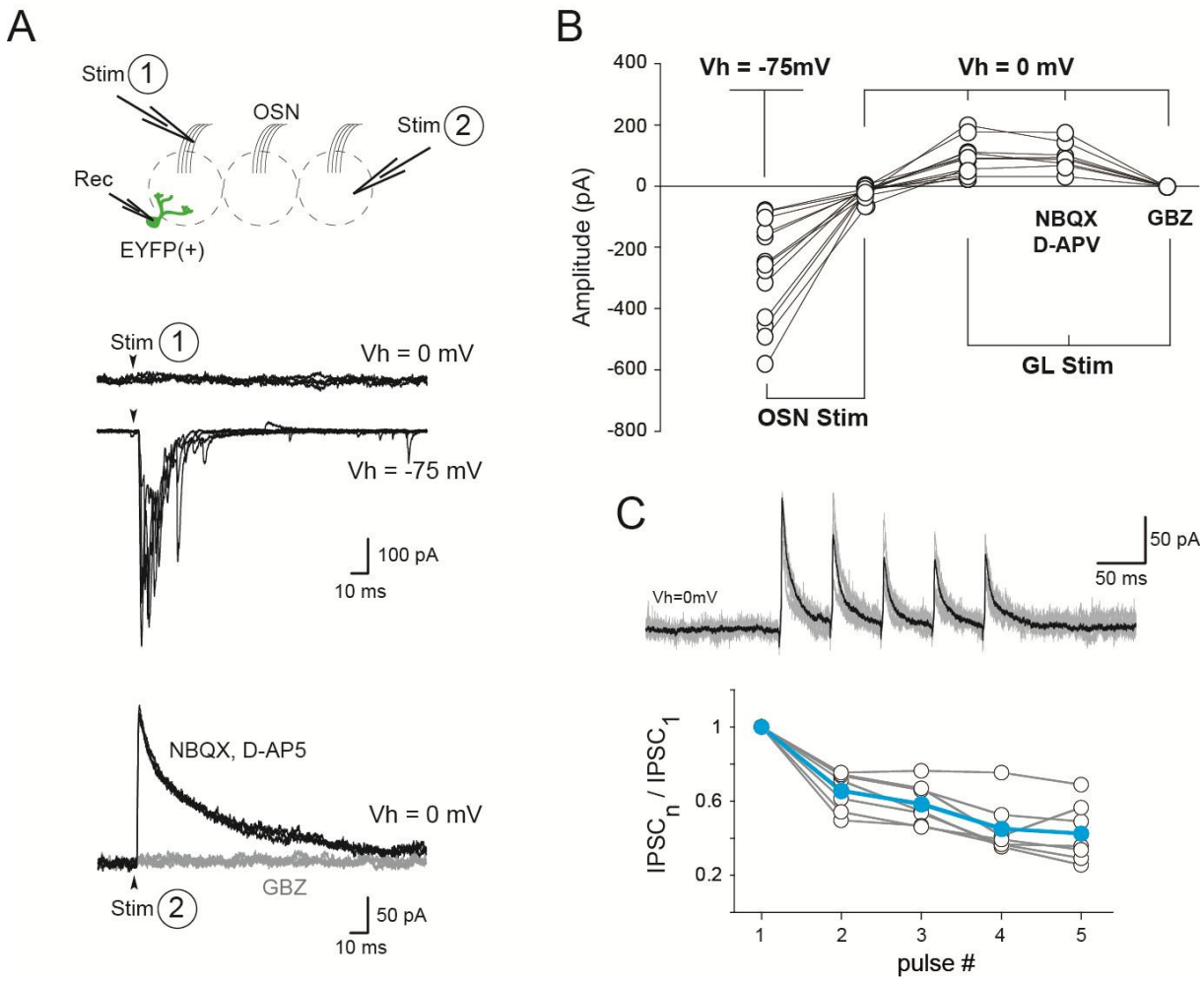

Figure 1 : Inhibitory inputs of Kv3.1-EYFP(+) type 2 PG cells are not mediated by the glomerular network. A, Synaptic responses of labeled type 2 PG cells in the Kv3.1-EYFP transgenic mouse in response to the stimulation of the OSN innervating their glomerulus (Stim 1, middle traces) or in response to a distant stimulation >200 µm away in the glomerular layer (Stim 2, bottom traces). EPSCs were recorded at Vh=-75 mV and IPSCs were recorded at Vh=0 mV. IPSCs evoked by stim 2 were recorded in the presence of NBQX (10 µM) and D-AP5 (50 µM) and were fully blocked by GBZ (5 µM, grey traces). **B,** Summary plot for all the EYFP(+) PG cells. **C,** Short-term depression of the inhibitory inputs of EYFP(+) PG Cells. Top, IPSCs evoked in a EYFP(+) PG cell by a 200 ms train of 20 Hz stimulations. The average trace (black) is superimposed on single responses (grey). Bottom, amplitude of the n^{th} IPSC normalized to the amplitude of the first IPSC (n=7). Blue plots show the average.

Spontaneous IPSCs were routinely observed in EYFP(+) PG cells indicating that the absence of any OSN-evoked IPSC does not reflect a lack of inhibitory synapses. Moreover, electrical stimulation in the glomerular layer at >200 µm away from the recorded PG cell evoked a reliable IPSC (n=16, average amplitude 87 ± 48 pA at Vh=0 mV) with a fast time course (decay time constant: 30 ± 13 ms, range 7.7-53.6 ms) that was blocked by the $GABA_A$ receptor antagonist gabazine (GBZ, 5 µM, Figure 1A and 1B). This evoked IPSC persisted in the presence of the AMPA and NMDA receptor antagonists, NBQX and D-AP5 respectively, demonstrating its monosynaptic nature (Figure 1A and 1B). In many cells the stimulus produced a composite IPSC with multiple peaks at distinct but reliable timing. These multiple peaks and the decrease of the response amplitude in stepwise manner with decreasing intensities of stimulation (supplementary Figure 2) suggest that stimulations in the glomerular layer can recruit several convergent inputs. To examine the short-term plasticity of this connection, we applied a train of five electrical stimuli delivered at 20 Hz. As illustrated in Figure 1C where the amplitude of the n^{th} IPSC relative to the first is plotted, the GABAergic IPSC strongly depressed ($IPSC_5/IPSC_1$ = 0.42 ± 0.16, n=7). All together, these results suggest that EYFP(+) PG cells receive inhibitory inputs from multiple long-range axonal projections ramifying in the glomerular layer of the olfactory bulb.

As labeled PG cells constitute only ~30% of all PG cells in the Kv3.1-EYFP mouse, we next repeated the same experiments in non-fluorescent PG cells. We have previously shown that a majority of EYFP(-) PG cells belongs to subclasses of type 2 PG cells (Najac et al., 2015). Similar to EYFP(+) PG cells, OSN stimulation did not evoke any IPSC in these diverse classes of EYFP(-) type 2 PG cells (n=23) whereas stimulation in distant glomeruli elicited a monosynaptic IPSC in the presence of NBQX and D-AP5 (n=12, mean amplitude 64 ± 47 pA; decay time constant: 16.0 ± 18.5 ms, range 6-70 ms)(Figure 2A, 2B). However, some PG cells

did receive IPSCs after OSN stimulations and they were all type 1 PG cells (seen in 8/18 type 1 PG cells, Figure 2C, 2D). These cells had a fast onset monosynaptic OSN-evoked EPSC at Vh= -75 mV and responded to a membrane supra-threshold depolarization with a train of spikes with accommodating amplitudes and sometime riding on the top of a calcium spike. At Vh= 0 mV, the inhibitory response was composed of multiple asynchronous IPSCs that were abolished in the presence of NBQX and D-AP5 (n=5) consistent with a plurisynaptic PG cell-mediated input generated within the glomerular network.

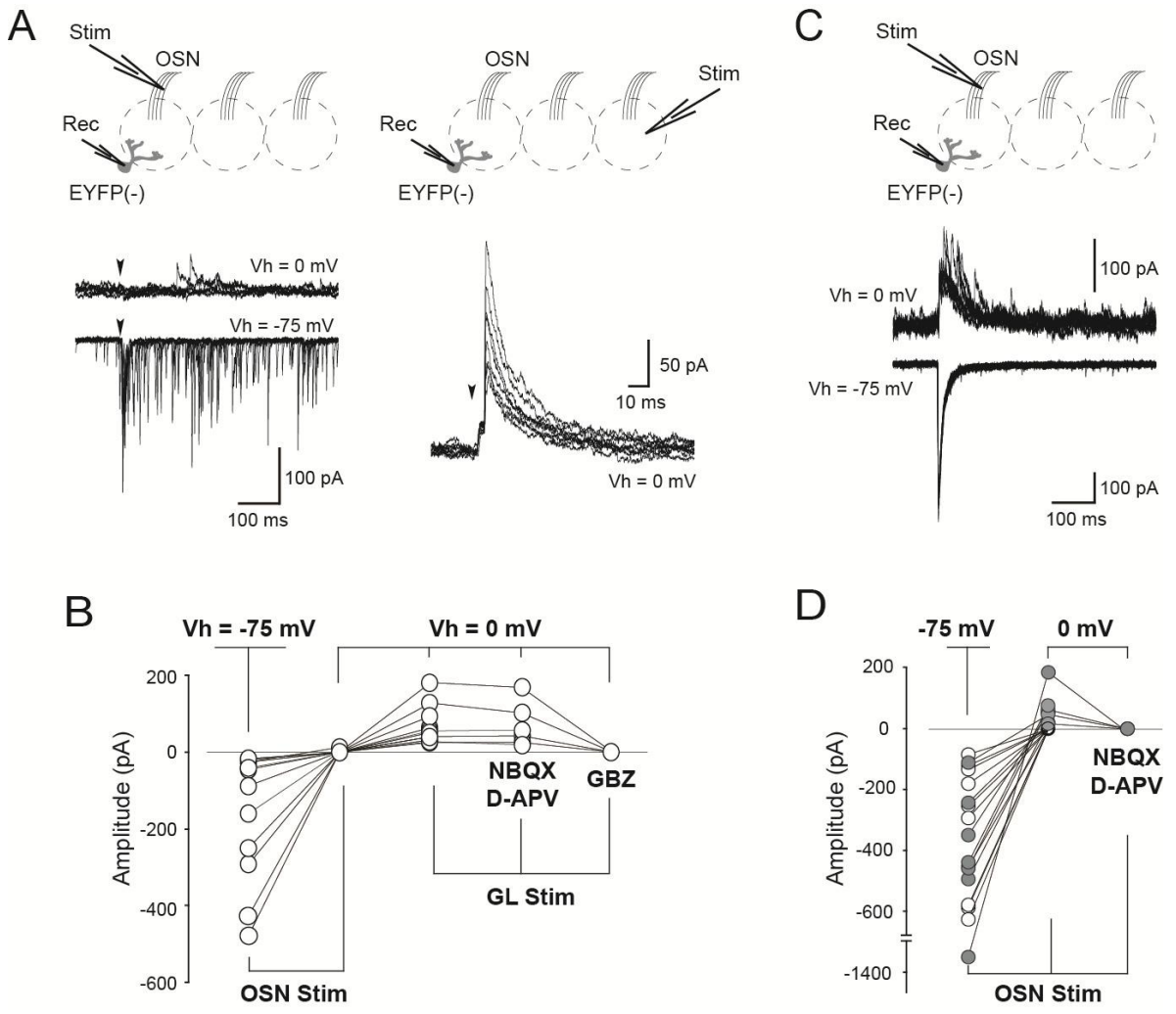

Figure 2 : Type 1 PG cells are the only PG cell subtype inhibited by other PG cells. **A,** Example of a type 2 PG cell, not labeled in the Kv3.1-EYFP mouse, that did not receive any OSN-evoked inhibitory input (left). In contrast, stimulation in distant glomeruli produced a robust ISPC (right). **B,** Summary plot for EYFP(-) type 2 PG cells tested in different stimulation and pharmacological conditions. **C,** Example of a type 1 PG cell responding to the stimulation of OSNs with a monosynaptic EPSC at Vh=-75 mV and with plurisynaptic IPSCs at Vh=0 mV. **D,** Summary plots for all type 1 PG cells tested. Cells with OSN-evoked IPSCs are shown in grey.

Long-range GABAergic projections innervate type 2 PG cells, granule cells and dSA cells

To further characterize PG cells GABAergic inputs, we next used the Thy1-ChR2-EYFP transgenic mouse expressing the light-gated Channelrhodopsin-2 (ChR2) fused to EYFP in numerous and diverse neuronal subtypes throughout the brain (Arenkiel et al., 2007). Although this mouse model is mostly known to express ChR2 in olfactory bulb mitral cells, we found that a brief (1-10 ms) blue light stimulation applied on olfactory bulb slices also evokes a monosynaptic GBZ-sensitive IPSC in about 25% of the PG cells tested. Light-evoked IPSCs had amplitudes ranging from few pA to several hundreds pA (average 156 ± 168 pA at Vh=0 mV, n=17), variable time courses (decay time constant from 6 to 168 ms, mean 37.9 ± 52 ms, Figure 3E) and were found in PG cells with diverse firing properties and OSN-evoked responses (Figure 3B). Yet, all responsive neurons were type 2 PG cells and none of the type 1 PG cells tested (n=11) responded to the photostimulation. Light-evoked IPSCs were resistant to NBQX and D-AP5 (n=9) consistent with a monosynaptic connection, but were abolished by TTX (1 µM) indicating that ChR2 activation must elicit a spike to induce GABA release (n=3). Similar to the electrically-evoked IPSCs, light-evoked IPSCs sometime displayed multiple peaks or bumps during the rising phase indicating that they resulted from summating asynchronous IPSCs (see the example in Figure 3B). Moreover, electrically-evoked IPSCs and light-evoked IPSCs had similar time course in cells in which the two stimuli were tested (n=4, not shown). Thus, in the Thy1-ChR2-EYFP mouse olfactory bulb, properties and targets of ChR2-expressing GABAergic fibers resemble those of the inhibitory fibers activated with an electrical stimulation in the glomerular layer.

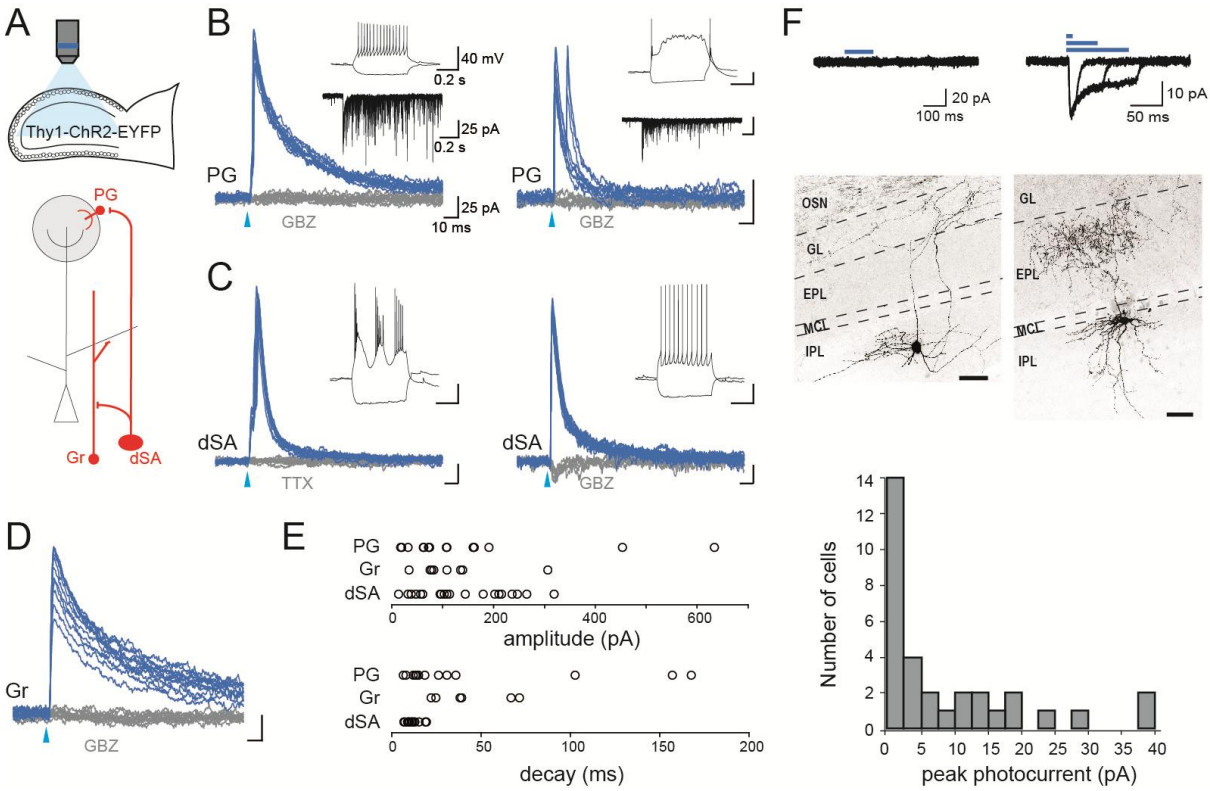

Figure 3 : GABAergic afferents to type 2 PG cells express ChR2 in the Thy1-ChR2-EYFP mouse. **A,** Circuit diagram of the three classes of interneurons tested in olfactory bulb slices from the Thy1-ChR2-EYFP transgenic mouse. **B,** Short blue light flashes (1-10 ms, blue arrowhead) evoked GBZ-sensitive IPSCs (blue traces) in different subtypes of type 2 PG cells. Insets show the intrinsic membrane properties (top) and OSN-evoked responses (bottom, Vh=-75 mV) of the two cells. Note that light sometime evoked pairs of IPSCs (right). **C,** Light-evoked IPSCs recorded at Vh=-75 mV in two deep SA (dSA) cells with distinct firing patterns. A small inward photocurrent persisted in the presence of GBZ in the cell shown on the right. **D,** light-evoked GBZ-sensitive IPSCs in a granule (Gr) cell. Scale bar values indicated in B apply for all traces in B, C and D. **E,** Light-evoked IPSC amplitudes (top) and decay time constants (bottom) in the three classes of interneurons. PG and granule cells were recorded at Vh=0 mV, dSA cells at Vh=-75 mV. **F,** dSA cells express little or no ChR2 in the Thy1-ChR2-EYFP mouse. Top, Light-evoked responses in two morphologically distinct dSA cells. Blue bars indicate the duration of the light stimulus. The cell on the right, with axonal ramifications in the external plexiform layer, express small ChR2-mediated photocurrents with durations depending on the stimulation duration. Bottom, summary histogram representing the maximal amplitudes of ChR2-mediated photocurrents in all the dSA cells recorded. Experiments were done at Vh=-75 mV, in the presence of GBZ, NBQX and D-AP5.

Interestingly, granule and dSA cells also received robust light-gated monosynaptic IPSCs in slices from the Thy1-ChR2-EYFP mouse (Figure 3C and 3D). In granule cells, light stimulation evoked GBZ-sensitive IPSCs in 8/19 cells tested. At Vh=0 mV and in the presence of NBQX and D-AP5, light-evoked IPSCs had an average amplitude of 120 ± 83 pA (range 34-307 pA) and a decay time constant of 41 ± 20.4 ms (range 22-71 ms)(Figure 3D). In dSA cells, flashes of light evoked a large ISPC in the majority of the cells tested (n=25/32)(Figure 3C). These IPSCs were sufficiently large to be visible at Vh=-75 mV, indicating a strong connection (average amplitude 139 ± 89 pA, range 14-319 pA, n= 20; at Vh=0 mV: amplitude range 80-

1564 pA, mean 707 ± 614 pA, n=5). Light-evoked IPSCs were found in dSA cells with diverse firing patterns (Figure 3C) and various axonal ramifications but were uniformly fast (decay time constant at Vh=-75 mV: 11.2 ± 3.5 ms, range 6.8-19.5 ms, n=20; at Vh=0 mV: 20.7 ± 11.2 ms, n=5). As in PG cells, light-evoked responses were abolished in the presence of TTX in both granule (n=3) and dSA cells (n=6). All together, these results suggest that a common GABAergic afferent expressing ChR2 in the Thy1-ChR2-EYFP mouse innervates all subtypes of type 2 PG cells, granule cells and the diverse subtypes of dSA cells.

Our data, together with previous reports (Eyre et al., 2008; Boyd et al., 2012; Burton et al., 2017), pointed to dSA cells as a likely candidate mediating inhibition of PG, granule and other dSA cells. To test this hypothesis, we examined light-gated photocurrents in dSA cells of the Thy1-ChR2-EYFP mouse using whole-cell recordings in the presence of NBQX, D-AP5 and GBZ (Figure 3F). Under these conditions, blue light stimulations did not induce any ChR2-mediated inward current in 13 over 32 dSA cells and only small light-gated currents in the remaining cells (n=19/32, averaged maximal current: 14.7 ± 11.4 pA). Moreover, light stimulation did not evoke firing in any of the cells tested in the cell-attached configuration before breaking in (n=20, not shown). Thus, even though some dSA cells weakly expressed ChR2, light-evoked depolarizations were likely too small to drive action potentials. The subset of recorded cells filled with biocytin (n=14) did not reveal a preferred expression of ChR2 in a specific dSA cell subtype. For instance, among the 5 dSA cells with visible axonal projections in the glomerular layer, only 2 had small light-gated currents (with maximal amplitudes of 10 and 5 pA). Furthermore, we did not observe any inward ChR2 mediated photocurrent across our multiple recordings in diverse types of neurons in the glomerular layer (that likely include PG and superficial SA cells) or in granule cells. Our results thus suggest that ChR2-expressing neurons that innervate PG, granule and dSA cells in the Thy1-ChR2-EYFP mouse likely reside outside the olfactory bulb.

As the principal source of centrifugal GABAergic afferents to the olfactory bulb is the HDB in the basal forebrain (Zaborszky et al., 1986; Gracia-Llanes et al., 2010; Niedworok et al., 2012), we next verified the expression of ChR2-EYFP in this region in fixed brains from the Thy1-ChR2-EYFP mouse. The basal forebrain of this mouse was indeed strongly fluorescent, especially in the HDB (n=4 mice, Supplementary Figure 3A). At the cellular level, the EYFP-coupled light-gated channel was expressed in a subset of HDB neurons co-

232 expressing GAD67 (32.4% of GAD67(+) neurons were ChR2-EYFP(+), n=712 GAD67(+) cells
233 counted, Supplementary Figure 3B). Thus, long-range GABAergic projections from the basal
234 forebrain may innervate the principal interneuron populations of the olfactory bulb.

235

236 **Selective expression of ChR2 in neurons of the HDB**

237 To further verify that GABAergic neurons from the HDB innervate olfactory bulb
238 interneurons, we injected an adeno-associated virus (AAV9) encoding a Cre-inducible ChR2-
239 EYFP in the basal forebrain of dlx5/6-Cre mice. These transgenic mice express the Cre
240 recombinase under the control of regulatory sequences of the dlx5/6 homeobox genes
241 exclusively in GABAergic neurons in the forebrain (Monory et al., 2006). Our viral injections
242 produced a strong EYFP labeling of fibers projecting to the olfactory bulb, especially in the
243 granule cell layer and in the glomerular layer (Figure 4A), similar as in a previous study using
244 a Cre-dependent viral approach in the GAD65-Cre mouse (Nunez-Parra et al., 2013). We then
245 tested the synaptic connections made by these ChR2-expressing HDB axons using whole-cell
246 voltage-clamp recordings in olfactory bulb slices. Activating ChR2-expressing axons with brief
247 (1-10 ms) flashes of blue light evoked large outward IPSCs in most PG (n=47/62, range 6-849
248 pA, mean 236 ± 222 pA at Vh=0 mV), granule (n=6/7, range 93-464 pA, mean 181 ± 143 pA at
249 Vh=0 mV) and dSA cells tested (n=7/7, range 241-681 pA, mean 416 ± 139 pA at Vh between
250 -15 and -35 mV)(Figure 4D and 4F). IPSCs were similar as those observed in the Thy1-ChR2-
251 EYFP mouse, i.e. they had diverse time course in PG cells (mean decay time constant 46.7 ±
252 56.9 ms, range 6-254 ms), they were fast in dSA cells (mean 12.8 ± 6.2 ms) and slightly
253 slower in granule cells (mean 32 ± 5 ms)(Figure 4F). Also consistent with the data obtained in
254 the Thy1-ChR2-EYFP mouse, light-evoked IPSCs were only observed in type 2 PG cells but not
255 in type 1 PG cells (n=0/5). In addition, responses were unaffected by the presence of NBQX
256 and D-AP5 (n=13), reversed at the expected equilibrium potential for chloride (ECl=-88 mV in
257 our recording conditions, n=8 PG cells, Figure 4E) and were totally abolished by GBZ (n=12
258 PG cells).

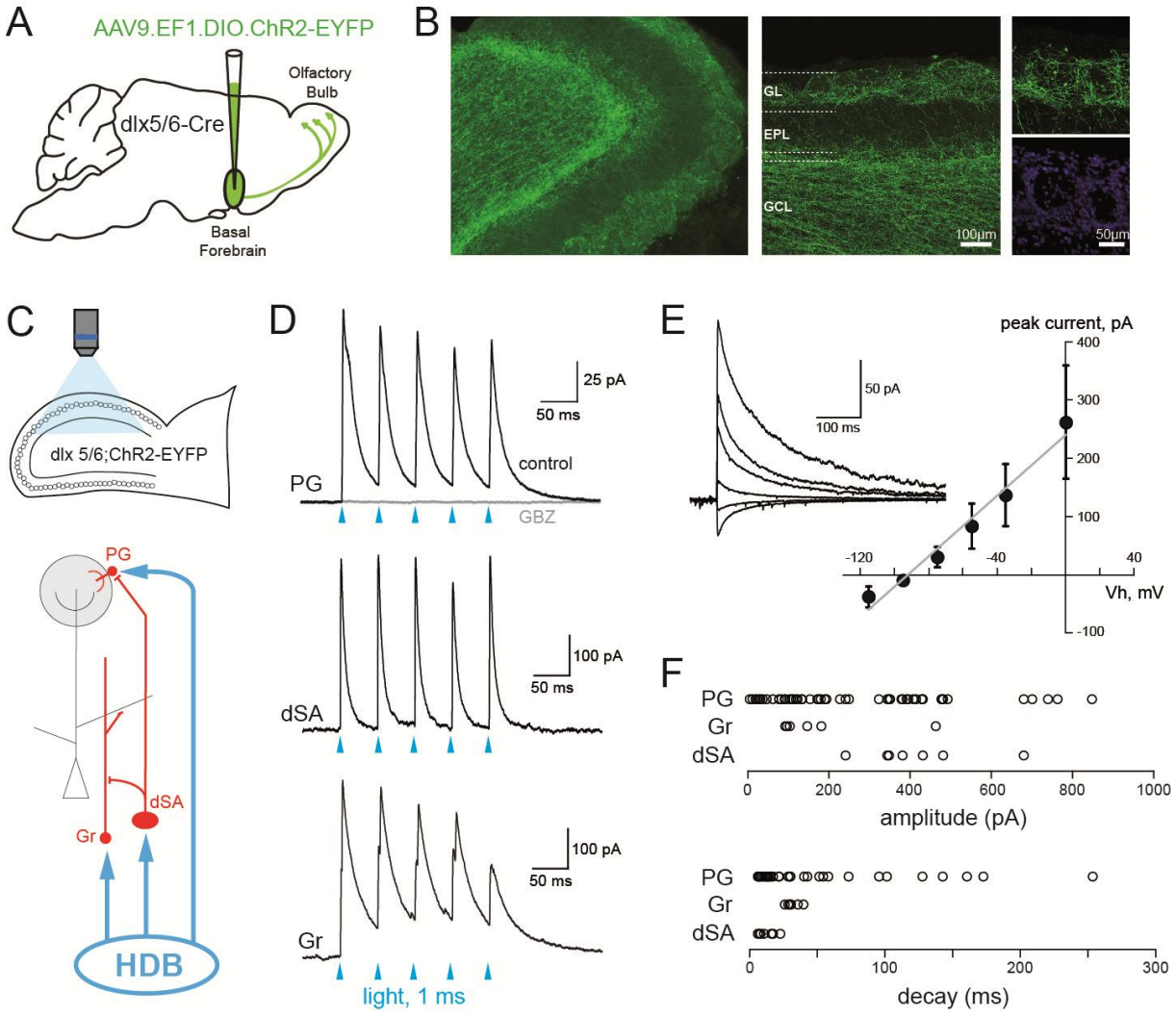

Figure 4 : Conditional expression of ChR2 in GABAergic neurons of the HDB demonstrates their connections with the major inhibitory interneurons of the olfactory bulb. A, Stereotaxic injection of a viral construct in the basal forebrain of dlx5/6-Cre mice was used for conditional expression of ChR2 in GABAergic neurons of the HDB. **B,** 3-5 weeks after injection, fibers expressing ChR2-EYFP were observed in all the layers of the olfactory bulb. The two images on the right are a zoom on two glomeruli (top ChR2-EYFP, bottom Hoechst staining). GL: glomerular layer, EPL: external plexiform layer, GCL: granule cell layer. **C,** Circuit diagram illustrating the direct synaptic connections of HDB fibers that were tested in dlx5/6-cre mice expressing ChR2 in the basal forebrain. **D,** Light-evoked IPSCs elicited in a PG cell (Vh=0mV, grey trace is in the presence of GBZ), a dSA cell (Vh=-15 mV) and in a granule cell (Gr, Vh=0 mV) in response to blue light flashes delivered at 20 Hz. Traces are average responses. **E,** Current-voltage relationship of the light-evoked IPSC in PG cells (n=8). Inset, IPSCs from a representative PG cell recorded at different holding potentials. **F,** amplitudes (top) and decay time constants (bottom) of light-evoked IPSCs recorded in PG, granule and dSA cells. PG and granule cells were recorded at Vh=0mV, dSA cells at Vh comprised between -35 mV and -15 mV.

Connection rates of ChR2-expressing fibers with type 2 PG cells were much higher in dlx5/6;ChR2-EYFP mice (>75%, n=47/62) than in the Thy1-ChR2-EYFP mouse, making it possible to examine this synaptic input by cell subtype (Figure 5). We classified, when possible, the responsive type 2 PG cells in the three previously described subgroups (Najac

et al., 2015), based on their membrane properties and OSN-evoked excitatory responses. Group 1 included cells with diverse firing patterns that responded to the stimulation of OSN with a short composite EPSC (average duration 38.5 ± 32 ms), similar as Kv3.1-EYFP(+) PG cells (Figure 5A). These cells had light-evoked responses (mean amplitude 152 ± 122 pA, n=8) with a decay time constant ranging from 6.7 to 51.2 ms (mean 25.2 ± 16.5 ms). Group 2 included cells with membrane and synaptic properties consistent with those of CR-expressing PG cells (i.e. firing at most one spike, receiving few spontaneous EPSC and small OSN-evoked inputs)(Figure 5B). Cells in group 2 received fast light-evoked IPSCs (average decay 12.8 ± 4.1 ms, average amplitude 353 ± 200 pA, n=15). In contrast, regular spiking PG cells with long-lasting (>100 ms) OSN-evoked responses (group 3, Figure 5C) had long light-evoked responses (average decay 102 ± 75 ms, amplitude 325 ± 316 pA, n=8). IPSC decay time constants in these three groups were statistically not equal (Kruskal-Wallis test, H=17.59, P= 0.00015). Decays in group 1 (Figure 5Aii) and group 2 (Figure 5Bii) were similar (p=0.14, Wilcoxon test) and faster than decays in group 3 (Figure 5Cii)(p=0.001 and p<0.0001, respectively, Wilcoxon test). In addition, trains of light-evoked IPSCs elicited at 20 Hz depressed at different degrees in the three groups as quantified by the paired-pulse ratio of the second IPSC amplitude relative to the first (Kruskal-Wallis test, H=12.60, p= 0.0018). Paired-pulse depression was stronger in group 1 (0.42 ± 0.16, n=6)(Figure 5Aiii) than in group 2 (0.73 ± 0.12, n=10; p=0.0005, Wilcoxon test) (Figure 5Biii) whereas the depression was intermediate in group 3 (0.52 ± 0.14, n=6, p=0.52 compared to group 1 and p=0.007 compared to group 2, Wilcoxon test)(Figure 5Ciii). Together, these data suggest that the properties of the HDB synaptic inputs are specific of the postsynaptic PG cell subtype.

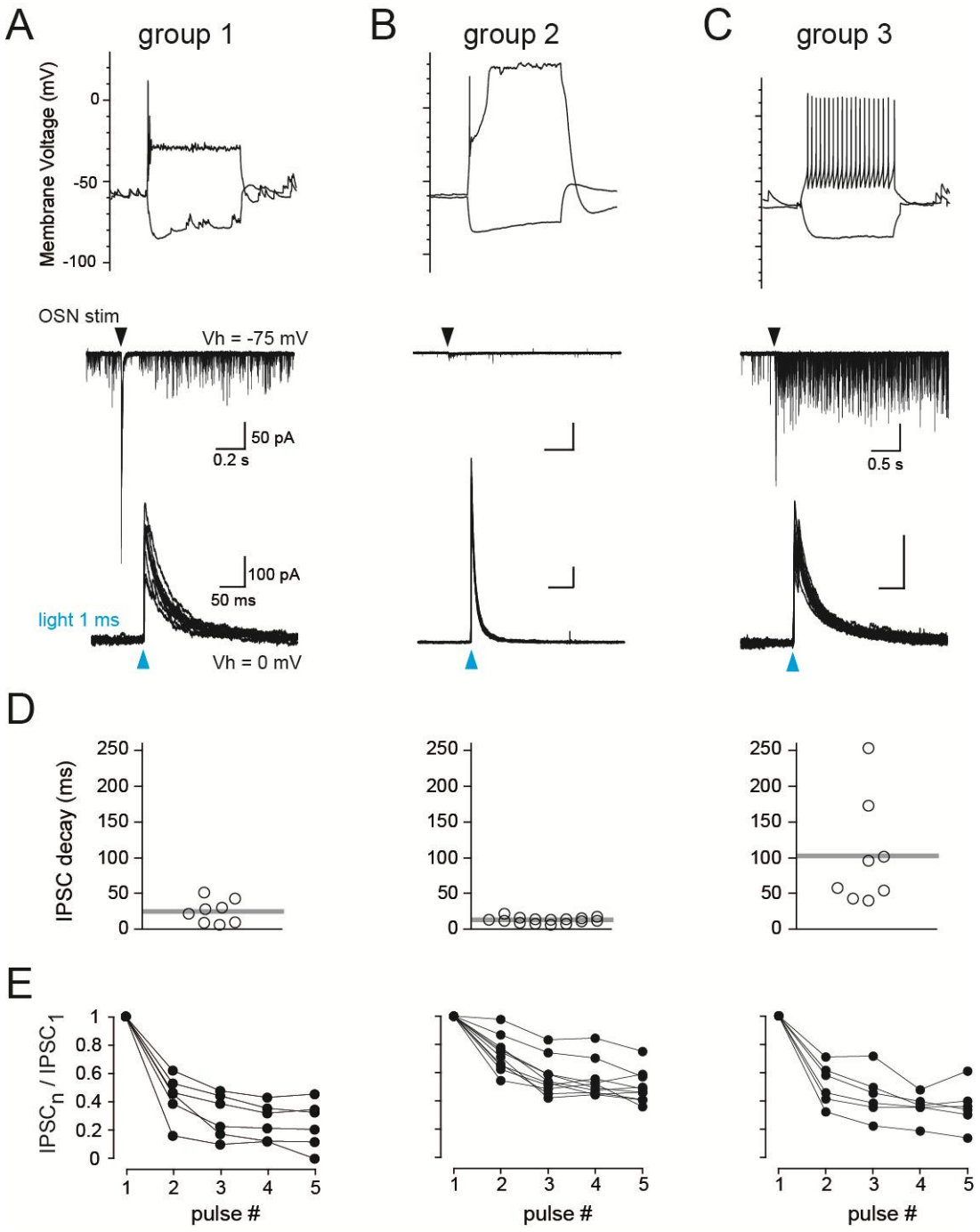

Figure 5 : GABAergic inputs from HDB fibers have different properties depending on the postsynaptic PG cell subtype. **A, B and C,** membrane potential responses to depolarizing and hyperpolarizing current injections (500 ms steps, top traces), OSN-evoked excitatory responses (middle traces) and light-evoked IPSCs in three PG cells representative of three subgroups of type 2 PG cells (A: group 1; B: group 2 and C: group 3). Cells were recorded in dlx5/6;ChR2-EYFP mice. Recording, stimulation conditions and scale bar values indicated in the first column apply for all, except where noted. **D,** decay time constants of light-evoked IPSCs in PG cells classified in the 3 subgroups of the corresponding column. Bars indicate the mean. **E,** amplitudes of the n^{th} light-evoked IPSC relative to the normalized amplitude of the first IPSC recorded in PG cells classified in the 3 subgroups of the corresponding column. Each cells was stimulated with 5 flashes of light at 20 Hz. Lines connect plots from the same cells.

311

312 **Functional implications of basal forebrain GABAergic inputs**

313 Previous studies found that the chloride concentration is high in PG cells and,
314 consequently, that GABA is depolarizing (Smith and Jahr, 2002; Parsa et al., 2015). The net
315 impact of GABA is, however, still unclear as one study concluded that GABA inhibits the firing
316 of PG cells by shunting excitatory inputs (Smith and Jahr, 2002) whereas the other found
317 that GABA is excitatory and induces the firing of PG cells (Parsa et al., 2015). To further
318 investigate this question, we examined the influence of light-evoked GABAergic synaptic
319 inputs on PG cells spiking activity in dlx5/6;ChR2-EYFP mice. Spontaneous firing was
320 monitored using loose cell-attached recordings and a short flash of light (1-10 ms) was
321 delivered every 2s. In a subset of cells, spontaneous firing was recorded in the cell-attached
322 configuration preceding whole-cell recordings.

323 Despite the high connection rate found in slices from dlx5/6;ChR2-EYFP mice, light
324 stimulation had no effect on a majority of the recorded PG cells (56/98 cells in loose cell-
325 attached recording). However, most of the non-responsive cells were totally silent or fired
326 only occasionally (n=37, 38%), so an inhibitory effect would be unnoticeable in these cells.
327 Only 19% of cells were insensitive while having a non-negligible firing activity (>1 Hz,
328 n=19/98). Light stimulations did influence the firing of 43% of the recorded PG cells (42/98
329 cells) in various ways, as illustrated in Figure 6. In a minority of cells (n=9, Figure 6A and 6B)
330 the light stimulus triggered a single spike. Yet, evoked spikes were precisely locked shortly
331 (<10 ms) after the light pulse, consistent with a direct depolarizing action of the GABA
332 postsynaptic current, in only 1 of these 9 cells (Figure 6A). In the 8 other cells, evoked spikes
333 occurred up to 570 ms after the light pulse and with less precision (jitters 20-50 ms)(Figure
334 6B), suggesting an indirect rebound excitation that was not further studied. Three cells that
335 responded to the light-evoked GABAergic input with a single spike were subsequently
336 characterized in the whole-cell configuration and had membrane and synaptic properties,
337 including fast light-evoked IPSCs (decay range 6-15ms), consistent with those of CR-
338 expressing cells (not shown).

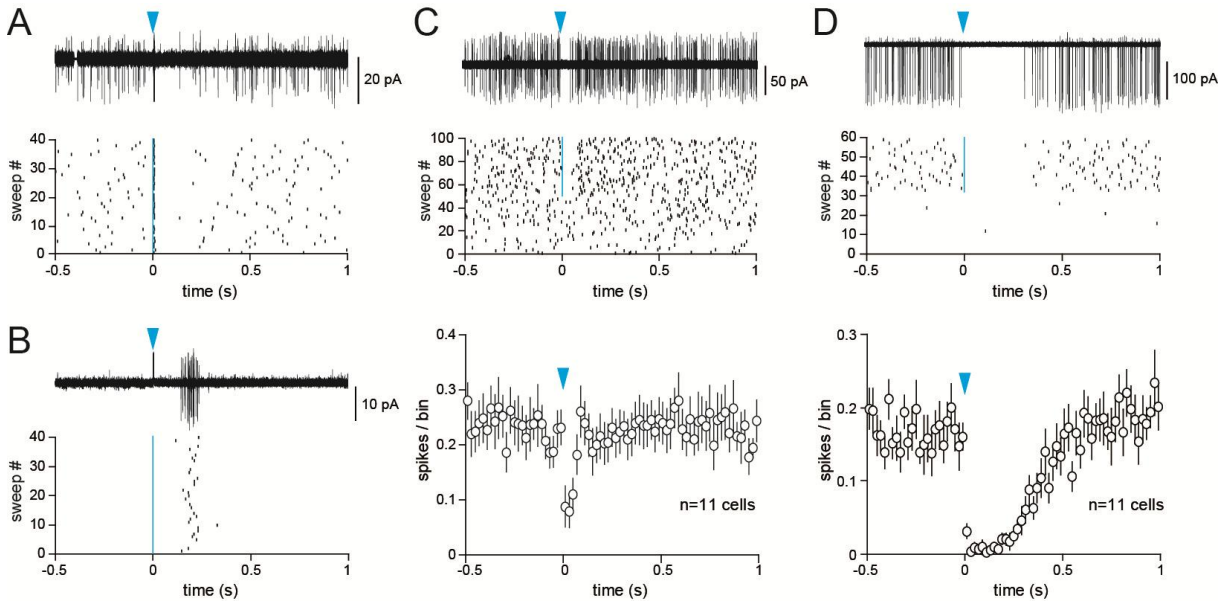

Figure 6 : GABAergic inputs from the HDB are excitatory or inhibitory in PG cells. A, loose cell-attached recording from a PG cell responding to the light flash (1 ms, blue arrow) with a single time-locked action potential. 30 superimposed episodes (top) and the corresponding raster plot (bottom) are shown. The light flash was applied at t=0 (vertical bar) every 2 s. **B,** example of a PG cell that fired a single and delayed action potential in response to the light stimulus. 22 superimposed episodes (top) and the corresponding raster plot (bottom) are shown. **C,** Top, loose cell-attached recording from a PG cell on which the light stimulus transiently blocked the firing. 30 superimposed episodes with light stimulation (arrow) and the corresponding raster plot are shown. Light stimulation (1 ms at t=0 every 2 s) started at episode 50. The summary plot shows the average number of spikes per 20 ms bin for n=11 PG cells. Bars show SEM. **D,** Top, loose cell-attached recording from a PG cell on which the light stimulus blocked the firing for a longer period of time. 29 superimposed episodes with light stimulation (arrow) and the corresponding raster plot are shown. Light stimulations (1 ms at t=0 every 2 s) started at episode 31. Note that this cell was almost silent before light stimulation started. The summary plot shows the average number of spikes per 20 ms bin for n=11 PG cells. Bars show SEM. Experiments were done in slices from dlx5/6;ChR2-EYFP mice.

The firing of 33 cells was, in contrast, inhibited by the light-evoked IPSC. This inhibition had variable time course across cells but two kinds of responses clearly emerged. In a first group of cells, light stimulation blocked the firing for a short period of time (first spike after the flash occurred at 105 ± 74 ms, n=11) without affecting the overall firing activity of the neuron (control spike frequency: 9.3 ± 5.5 Hz; during light stimulations: 9.5 ± 5.1 Hz, paired Student's *t*-test p=0.824)(Figure 6C). Only one cell showing this transient inhibition of spiking could be characterized in the whole-cell configuration. It had a short OSN-evoked excitatory response and emitted several spikes demonstrating that it was not a CR-expressing PG cell (not shown).

In a second group, cells were inhibited for a longer period of time (first spike after the flash occurred at 421 ± 161 ms, n=15) and, as illustrated in Figure 6D, surprisingly started to

fire at a higher rate after the first pulses of light. To further understand this excitatory effect of the light flashes, we stimulated the same cells at a lower frequency (every 15-20 s). This revealed that stimulation of HDB fibers caused a robust (>4 fold firing rate increase relative to baseline) and sustained rebound excitation that peaked ~1 s after the flash of light (Figure 7A and 7B). Importantly, this rebound excitation always followed a pause of firing. This dual response was observed in n=15 PG cells, sometime in the same slices as the shorter spiking inhibition seen in other cells (Figure 7C) suggesting that these different responses do not reflect discrepancies of viral infection between mice. GBZ abolished the pause of firing but had no effect on the rebound excitation (n=6/6 cells, Figure 7C). In contrast, the muscarinic ACh receptor antagonist atropine (10 µM) abolished the rebound excitation (n= 4/4 cells) without affecting the pause of firing (as seen in 2 cells, the 2 others cells stopped firing in the presence of atropine)(Figure 7D).

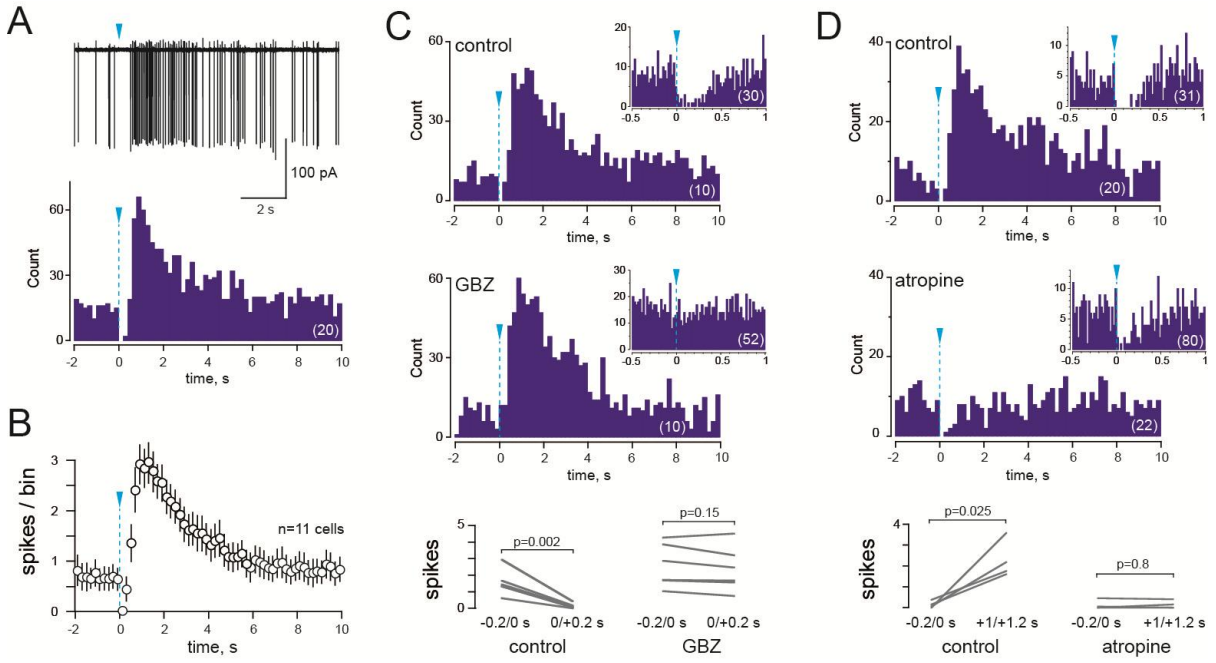

Figure 7 : Double inhibitory-excitatory effect of basal forebrain inputs. A, loose cell-attached recording of a PG cell responding to a short light stimulation (1 ms, arrow) with a pause of firing followed by an increase of firing. The corresponding distribution histogram shows the summed numbers of spikes (bin size = 200 ms) during 20 consecutive trials as indicated by the number within parenthesis. Light stimulation at t=0. **B,** Summary data for 11 cells responding to the light stimulus with a double inhibitory-excitatory effect. Plots represent the average number of spikes per 200 ms bin. Bars show SEM. Light (1-10 ms at t=0, blue arrow) was applied every 15-20s. **C,** GBZ (5µM) blocked the initial pause of firing without affecting the rebound excitation. Spike distribution histograms are from the same cell stimulated every 15 s (bin 200 ms) or every 2 s (insets, bin 20 ms) in control condition and in the presence of GBZ. Bottom, summary data for 6 cells recorded in control condition (left) and in the presence of GBZ (right). Average numbers of spikes within the 200 ms preceding the light flash (-0.2/0 s) and within the 200 ms period following the flash (0/+0.2 s) were compared with the paired

Student's *t*-test. **D,** Atropine (10µM) blocked the rebound excitation without affecting the initial pause of firing. The histograms are from the same cell stimulated every 15 s (bin 200 ms) or every 2 s (insets, bin 20 ms) in control condition and in the presence of atropine. Bottom, summary data for 4 cells recorded in control condition (left) and in the presence of atropine (right). Numbers of spikes within the 200 ms preceding the light flash (-0.2/0 s) and within the 1/1.2s period following the flash were compared with the paired Student's *t*-test.

Finally, 6 PG cells responding with a long-lasting spiking inhibition in cell-attached (first spike after the flash occurred at 527 ± 263 ms) were characterized with whole-cell recordings. All these cells had a regular firing, long-lasting OSN-evoked excitatory responses (duration > 100 ms) and long light-evoked IPSCs (decay range 54-253 ms) and thus belonged to the group 3 of type 2 PG cells (Figure 8). In these cells, the frequency of spontaneous EPSCs was reduced for several hundreds of milliseconds following light-evoked IPSCs (Figure 8C), consistent with an inhibition of mitral and tufted cells output. This further argues that the acetylcholine-mediated rebound increase in firing was not caused by an indirect network-driven excitation. Thus, our data suggest that HDB fibers release both GABA and ACh on a specific PG cell subtype. Whether these two neurotransmitters are released at the same synapses and are packed in the same vesicles was not further studied here.

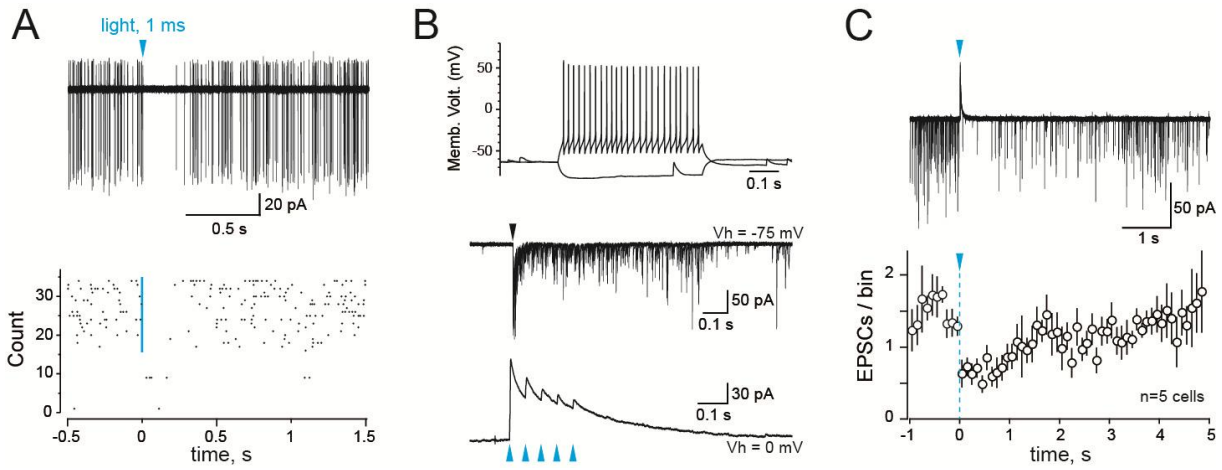

Figure 8 : Functional properties of PG cells with a dual inhibitory-excitatory response to basal forebrain inputs. A, cell-attached recording from a PG cell on which a light flash (1 ms, blue arrow) caused a dual response. The 16 superimposed traces show the pause of firing induced by the light stimulus. The corresponding raster plot (bottom) shows that the cell was almost silent before the first light stimuli (at t=0 every 2 s starting at episode 16). **B,** Membrane potential responses, OSN-evoked excitatory responses (middle) and light-evoked IPSCs (bottom, 5 flashes at 20 Hz) in the same cell as in A. **C,** In cells with similar functional profiles as in B, spontaneous EPSCs were less frequent following the light-evoked IPSC. 5 superimposed whole-cell current traces from one representative PG cell illustrate this reduced EPSC frequency. The Summary plot represents EPSC probability ± SEM per 100 ms bin from 5 cells. Light-stimulation at t=0.

Together, our results indicate that centrifugal GABAergic fibers originating from the basal forebrain have multiple interneuronal targets in the olfactory bulb and diverse

properties and functional impacts that largely depend on the postsynaptic cell subtype they connect with.

Discussion

Most efforts in understanding the function of olfactory bulb inhibition have focused on the local activation mechanisms of the diverse interneuron populations and on the impact of their activity in shaping the olfactory bulb output. In comparison, GABAergic circuits that control the activity of olfactory bulb interneurons have received little attention. We show here that long-range GABAergic projections from the basal forebrain make prominent connections on many classes of interneurons in the olfactory bulb with a previously unsuspected level of synaptic complexity. These data reinforce the idea that the basal forebrain is a major modulator of olfactory bulb circuits and suggest that understanding its global impact on olfactory processing will require a careful and differential investigation of its action on each targeted neuronal subtype in the olfactory bulb.

The basal forebrain sends massive cholinergic and GABAergic fibers to the olfactory bulb

The basal forebrain contains several nuclei without clear delineations that innervate the cerebral cortex, limbic areas, hippocampus, thalamic structures and the olfactory bulb with cholinergic and GABAergic projections. In the bulb, cholinergic projections from the HDB are found essentially in the glomerular layer and in the internal plexiform layer and, moderately, in the granule cell layer (Macrides et al., 1981; Zaborszky et al., 1986; Salcedo et al., 2011; Case et al., 2017; Hamamoto et al., 2017). The HDB sends even more massive GABAergic projections in all layers of the bulb (Zaborszky et al., 1986; Gracia-Llanes et al., 2010; Niedworok et al., 2012; Nunez-Parra et al., 2013). These two neural populations are not clearly segregated in the HDB (Zaborszky et al., 1986) and many neurons in the basal forebrain express the molecular machinery to co-transmit GABA and ACh (Saunders et al., 2015; Case et al., 2017) illustrating how intricate these two centrifugal pathways are.

Basal forebrain cholinergic signaling modulates odor detection, discrimination and olfactory learning (Ma and Luo, 2012; Devore et al., 2014; Rothermel et al., 2014). The underlying cellular mechanisms are, however, still unclear because ACh modulates diverse OB neurons at different timescales, via multiple pre- and postsynaptic muscarinic and

nicotinic receptors and with apparently divergent actions (Castillo et al., 1999; Ghatpande and Gelperin, 2009; Liu et al., 2015; Smith et al., 2015). Selective pharmacological inactivation of HDB GABAergic neurons using a DREADD/CNO paradigm also impairs olfactory sensitivity and odor discrimination (Nunez-Parra et al., 2013). Our data demonstrating that GABAergic HDB fibers have multiple targets in the bulb together with recent results demonstrating ACh and GABA co-transmission from some HDB fibers suggest that these two centrifugal pathways are intimately coupled and that their influence cannot be inferred independently.

Long-range GABAergic projections from the basal forebrain regulate diverse interneuron populations in the olfactory bulb

We here report the connections of HDB fibers with PG cells, dSA cells and granule cells that, together, constitute the main populations of interneurons in the bulb. The goal of our study was not to provide an exhaustive description of HDB GABAergic neuronal targets in the olfactory bulb. Thus, we did not test principal neurons, superficial SA cells or interneurons located in the EPL that are putative targets as well. Instead, we concentrated our study on PG cells to illustrate the complexity of long-range GABAergic projections and their fine regulation of local interneurons activity. We show that HDB fibers elicit IPSCs with distinct time courses and short term plasticities in the three functionally different subgroups of type 2 PG cells we previously described (Najac et al., 2015). Group 1 is composed of various PG cells and includes CB-expressing cells, group 2 corresponds to CR-expressing PG cells and group 3 is formed by regular firing neurons with long-lasting OSN-evoked excitatory response. GABAergic connections are an additional criterion that helps classifying these diverse PG cell subtypes. IPSCs with diverse durations likely reflect different subunit compositions of postsynaptic $GABA_A$ receptors. For instance, the selective expression of the alpha5 subunit in a PG cell subpopulation that does not overlap with CB- and CR-expressing PG cells (Panzanelli et al., 2007) might correlate with slow IPSCs and prolonged firing inhibition in PG cells of group 3.

Postsynaptic $GABA_A$ receptors with different kinetics also contribute in shaping short term depression. However, the different degrees at which IPSCs depressed in PG cells may also reflect presynaptic diversity. Thus, distinct subset of chemically-defined HDB GABAergic neurons may have spatially defined projections in the olfactory bulb and control specific

postsynaptic bulbar interneurons. In support with this hypothesis, we found evidence of ACh/GABA co-transmission in only one selective subgroup of PG cells. On these particular PG cells, ACh activates a muscarinic receptor that produces a long-lasting excitation which likely triggers the release of GABA onto mitral cells, as previously suggested (Liu et al., 2015). Only a fraction of HDB GABAergic neurons co-express markers of cholinergic transmission (Saunders et al., 2015). Among those, another specific subset preferentially projects in the internal plexiform layer of the olfactory bulb where it selectively connects with dSA cells (Case et al., 2017). Recent immunostaining experiments also highlight the chemical diversity of HDB GABAergic neurons, each subtype making specific connections in multiple regions of the brain (Do et al., 2016). Thus, addressing the synaptic complexity of HDB GABAergic inputs in the olfactory bulb may necessitate the use of transgenic mice allowing the manipulation of genetically-identified population of HDB neurons.

Basal forebrain projections control type 2 PG cells

We found that HDB fibers contact the different subtypes of type 2 PG cells but not type 1 PG cells. We also show that type 2 PG cells do not receive synaptic inputs from other PG cells whereas type 1 PG cells do. A previous study described GABAergic interactions in pairs of unidentified PG cells projecting within the same glomerulus (Murphy et al., 2005). This GABAergic signaling requires the activation of an L-type mediated calcium spike in the presynaptic PG cell and induces a slow composite postsynaptic IPSC, suggesting that PG-PG cells interactions rely on GABA spillover (Smith and Jahr, 2002). In contrast, and consistent with our results, fast sodium action potentials in the presynaptic PG cell fail to evoke any IPSC. In our experiments, we used OSN stimulation to induce burst of action potentials in PG neurons (Najac et al., 2015). However, even high intensity of stimulations failed to evoke IPSCs in type 2 PG cells whereas they were evoked in type 1 PG cells. Thus, our results and those of Murphy et al. suggest that local PG-PG cells synaptic interactions are restricted to type 1 PG cells.

Deep SA cells also provide inhibitory input on type 2 PG cells. Ultrastructural examination of dSA cell terminals demonstrated that CB-expressing PG cells are among their postsynaptic targets (Eyre et al., 2008). Moreover, Burton et al. recently reported that optical activation of dSA cells elicits a monosynaptic IPSC on diverse type 2 PG cells (Burton et al., 2017). Our data do not contradict these previous results but show that other circuits

514 regulate PG cells as well. However, dSA cells being themselves modulated by HDB inputs, our
515 results strongly suggest that centrifugal HDB fibers exert a fine control of intraglomerular
516 inhibition mediated by type 2 PG cells.

517 We found that the principal impact of basal forebrain GABAergic synaptic inputs was to
518 inhibit the firing of PG cells. Only one cell over nearly 100 tested responded with a time-
519 locked action potential consistent with a GABA-induced firing. This might seem surprising as
520 previous report indicate that GABA is depolarizing in PG cells (Smith and Jahr, 2002; Parsa et
521 al., 2015). However, depolarizing HDB inputs may shunt excitatory signals, as previously
522 shown (Smith and Jahr, 2002). Also, our results were all obtained in adult mice whereas
523 those of Parsa et al. and Smith et al. were mostly obtained in slices from young (12-17 days
524 old) mice or rats in which immature cells with high intracellular concentration of chloride
525 might be overrepresented. Finally, our experiences also suggest that the basal forebrain
526 input directly or indirectly inhibits mitral and tufted cells, thus reducing their glutamatergic
527 output onto PG cells. Regardless of the underlying mechanism, our results highlight that
528 basal forebrain inputs have multiple and complex target-specific impacts in the glomerular
529 network.

530

531 **Role of HDB centrifugal afferents in olfactory bulb odor processing**

532 The diversity of olfactory bulb interneurons under the control of HDB fibers makes it
533 challenging to predict the global functional implications of this GABAergic innervation on the
534 olfactory bulb output. In the simplest way, inhibition of olfactory bulb interneurons may
535 induce a disinhibition of mitral and tufted cells and thus facilitate the olfactory bulb output.
536 However, the direct or indirect excitatory action of GABAergic IPSCs and the co-transmission
537 of GABA and ACh on, at least, some interneurons, complicate this view. Moreover, as
538 olfactory bulb processing is fundamentally rhythmic and tightly coupled to the respiration,
539 the physiological impact of HDB centrifugal inputs may depend on their temporal dynamics
540 along a respiration cycle. A synchronized activity of these centrifugal afferents may reset the
541 activity of olfactory bulb circuits before a new respiration cycle. But how synchronized are
542 they? Recent data indicate that non-cholinergic neurons in the HDB have their activity
543 correlated with attention whereas the activity of cholinergic neurons is correlated with
544 primary reinforcers and outcome expectations (Hangya et al., 2015). Centrifugal inputs from

545 the HDB could therefore contextually modulate the olfactory bulb activity as a function of
546 the internal state.

547 Interestingly, HDB GABAergic fibers and axonal feedback from the olfactory cortex
548 target the same populations of interneurons in the bulb. Thus, axons from pyramidal cells of
549 the piriform cortex or the anterior olfactory nucleus directly excite olfactory bulb
550 interneurons and facilitate mitral cell inhibition (Boyd et al., 2012; Markopoulos et al., 2012),
551 i.e. the exact opposite of what HDB GABAergic fibers might do. Cortical feedback exerts
552 spatially diffuse, temporally complex and non-uniform actions on olfactory bulb
553 interneurons in response to odors (Boyd et al., 2015; Otazu et al., 2015). Because functional
554 (Paolini and McKenzie, 1997; Linster and Hasselmo, 2000) and anatomical (Do et al., 2016)
555 evidence suggest that HDB neurons receive inputs from pyramidal cells of the olfactory
556 cortex, it will be important to determine the relative timing of cortical feedback and HDB
557 fibers inputs and if these two pathways balance each others on the same postsynaptic
558 bulbar interneurons or instead have opposite actions on different ensemble of interneurons.
559

560 **Materials and Methods**

561 *Animals*. All experimental procedures were approved by the French Ministry and the local
562 ethic committee for animal experimentation (C.R.E.M.E.A.S). Three transgenic mouse lines
563 were used. Kv3.1-EYFP mice express the enhanced yellow fluorescent protein (EYFP) under
564 the control of the Kv3.1 K^+ channel promoter (Metzger et al., 2002). Thy1-ChR2-EYFP mice
565 express channel-rhodopsin 2 (ChR2) fused to EYFP under the control of the thymocyte
566 antigen 1 (Thy1) promoter (B6.Cg-Tg (Thy1-COP4/EYFP) 18 Gfng/J from the Jackson
567 laboratory, Bar Harbor, ME)(Arenkiel et al., 2007). Dlx5/6-Cre mice express the Cre
568 recombinase under the control of the regulatory sequences of the dlx5 and dlx6 genes
569 (Monory et al., 2006).

570 *Slice preparation.* 3 weeks to 3 month-old mice of either sex were killed by decapitation and
571 the olfactory bulbs rapidly removed in ice-cold oxygenated (95% O2-5% CO2) solution
572 containing (in mM): 83 NaCl, 26.2 NaHCO3, 1 NaH2PO4, 2.5 KCl, 3.3 MgSO4, 0.5 CaCl2, 70
573 sucrose and 22 D-glucose (pH 7.3, osmolarity 300 mOsm/l). Horizontal olfactory bulb slices
574 (300 µm) were cut using a Microm HM 650V vibratome (Microm, Germany) in the same

575 solution; incubated for 30-40 minutes at 34°C; stored at room temperature in a regular
576 artificial cerebrospinal fluid (ACSF) until use. ACSF contained (in mM): 125 NaCl, 25 NaHCO3,
577 2.5 KCl, 1.25 NaH2PO4, 1 MgCl2, 2 CaCl2 and 25 D-glucose and was continuously bubbled
578 with 95% O2-5% CO2.

579 *Electrophysiological recordings.* Experiments were conducted at 32-34°C under an upright
580 microscope (SliceScope, Scientifica, Uckfield, UK) with differential interference contrast (DIC)
581 optics. Whole-cell recordings were made with glass pipettes (3-6 MΩ) filled with a K-
582 gluconate-based internal solution containing (in mM): 135 K-gluconate, 2 $MgCl_2$, 0.025 $CaCl_2$,
583 1 EGTA, 4 Na-ATP, 0.5 Na-GTP, 10 Hepes (pH 7.3, 280 mOsm). Atto 594 (10 µM, Sigma) was
584 added to the internal solution in order to visualize the cell morphology. Loose cell-attached
585 recordings (15-100 MΩ seal resistance) were made with pipettes filled with ACSF. OSN axons
586 bundles projecting inside a given glomerulus were electrically stimulated using a theta
587 pipette filled with ACSF as previously described (Najac et al., 2015). The electrical stimulus
588 (100 µs) was delivered using a Digitimer DS3 (Digitimer, Welwyn Garden City, UK). Optical
589 stimulation was done through a blue (490 nm) CoolLED pE 100 (CoolLED Ltd., Andover, UK)
590 directed through the 40X objective of the microscope. Recordings were acquired with a
591 multiclamp 700B amplifier (Molecular Devices, Sunnyvale, CA), low-passed filtered at 2-4 kHz
592 and digitized at 10 kHz using the AxoGraph X software (Axograph Scientific). In current-
593 clamp recordings, a constant hyperpolarizing current was injected in order to maintain the
594 cell at a potential of -60/-70 mV. In voltage-clamp recordings, access resistance (Ra<30 MΩ
595 for PG, granule and deep SA cells) were not compensated. Voltages indicated in the paper
596 were corrected for the junction potential (-15 mV).

597 *Drugs.* 6-nitro-7-sulfamoylbenzo[f]quinoxaline-2,3-dione (NBQX), D-2-Amino-5-
598 phosphonopentanoic acid (D-AP5), 2-(3-carboxypropyl)-3-amino-6-(4
599 methoxyphenyl)pyridazinium bromide (GBZ) were purchased from Abcam Biochemicals,
600 atropine from Sigma-Aldrich and tetrodotoxin (TTX) from Alomone labs.

601 *Cell morphology.* To reconstruct the morphology of the recorded cells, biocytin or
602 neurobiotin (Sigma-Aldrich) was added to the intracellular solution (1mg/ml). The patch
603 pipette was slowly withdrawn after the recordings to avoid damaging the cell bodies. Slices
604 were then fixed in 4% paraformaldehyde overnight, washed 3 times and incubated in a

permeabilizing solution containing Cy-5 conjugated streptavidin (1 µg/ml; Thermo Fischer) overnight. After 3 wash cycles with PBS, sections were mounted. Labeled cells were imaged with a confocal microscope (Leica TCS SP5).

Stereotaxic viral injections. 3-6 weeks old dlx5/6-cre transgenic mice were anesthetized with intraperitoneal injection of ketamine (20%), acepromazine (6%) and medetomidine (11.8%) mix (100µl/10g) and placed in a stereotaxic apparatus. Mice were craneotomized and a volume of 200-500 nl of AAV9.EF1a.DIO.hChR2(H134R).eYFP.WPRE.hGH (University of Pennsylvania Viral Vector Core) was stereotaxically injected with a Pneumatic Picopump PV 820, at 0.2 mm AP, -1.6 mm ML and -5.75 mm DV from bregma. After surgery, mice were injected with Metacam 100 (meloxicam) (5%) (100µl/10g), Antisedan (atipamezol) (2.5%) (100µl/10g), rehydrated with 1 ml of NaCl 0.9% and placed under a heating lamp. Mice recovered during 3-4 weeks after injection before anatomical or physiological experiments.

Analysis. EPSCs, IPSCs or photocurrent amplitudes were measured as the peak of an average response computed from multiple sweeps. The decay of light-evoked IPSCs was most often best fitted with a double exponential with time t=0 at the peak of the current. Time constant values indicated in the text are weighted decay time constant calculated using the following equation: $\tau_w = (\tau_1 A_1 + \tau_2 A_2)/(A_1 + A_2)$ where τ_1 and τ_2 are the fast and slow decay time constants and A_1 and A_2 are the equivalent amplitude weighting factors. Action potential capacitive currents recorded in loose cell-attached were automatically detected by the Axograph X software using an amplitude threshold. PSTH (peri stimulus time histograms) representing the cumulative number of action currents per 20 ms or 200 ms bin across several consecutive sweeps or the average number of spikes/bin/sweep were then constructed. To estimate the duration of an OSN-evoked plurisynaptic excitatory response, individual EPSCs with amplitude >5 pA were automatically detected by the Axograph X software using a sliding template function. PSTH representing the cumulative number of EPSCs per 20 ms bin across several consecutive sweeps were then constructed. The decaying phase of these histograms was fitted with a single or with two exponentials to provide a time constant of the OSN-evoked response duration.

Statistics. Data are expressed as mean ± SD unless otherwise specified in some graphs. We used the Student's *t*-test to assess the statistical difference between paired sets of data with

normal distribution, the non-parametric Wilcoxon-Mann-Whitney rank sum test to assess the statistical difference between unpaired sets of data, the Kruskal-Wallis test for data sets with more than two variables and p-values are reported.

Immunohistochemistry. Adult mice (1-3 months) were deeply anesthetized with intraperitoneal injection of xylazine (6.3%) and ketamine (25%) and intracardially perfused with 4% paraformaldehyde (PFA). Brains were removed and kept in 4% PFA overnight. Slices were cut (50 µm thick) with a vibratome (Leica VT 1000S). Blocking steps were performed using a PBS solution containing 2% BSA and 0.3% Triton X-100 during 2h. Sections were incubated overnight at 4°C with mouse anti-GAD67 (1:500, Chemicon). After three washes in PBS, they were incubated 2 hours at room temperature with secondary antibodies—Alexa fluor 555 or Alexa fluor 633 anti-mouse (1:200, Molecular Probes, Eugene, OR). After three washes, sections were incubated with Hoechst staining (1:1000, 30 min) and finally mounted in Prolong Diamond Antifade Mountant (Molecular Probes). Images were taken using a Leica TCS SP5 II confocal microscope or an Axio Imager M2 for mosaic images. Immunostained and EYFP-expressing cells were manually counted using Cell counter plug-in on Fiji software.

Acknowledgements

This work was supported by the Centre National pour la Recherche Scientifique, the Université de Strasbourg and the Agence Nationale pour la Recherche (Grant ANR-12-JSV4-006-01). ASD was funded by a fellowship from the Ministère de la Recherche and by a fellowship from the Fonds Paul Mandel pour les Recherches en Neuroscience. We thank Ipek Yalcin (Institut des Neurosciences Cellulaires et Intégratives, Strasbourg) and Claire Gaveriaux-Ruff (Institut de Génétique et de Biologie Moléculaire et Cellulaire, Strasbourg) for the kind gift of the dlx5/6-Cre mice and Thomas Knöpfel (Imperial College, London) for the kind gift of the Kv3.1-EYFP mice. We thank Sophie Reibel-Foisset and the animal facility Chronobiotron (UMS 3415 Centre National pour la Recherche Scientifique and Université de Strasbourg), the Plateforme Imagerie In Vitro-Neuropôle-Strasbourg, and Aline Huber for their technical assistance. We thank Jean Christophe Cassel (Laboratoire de Neurosciences Cognitives et Adaptatives, Strasbourg) Nuria Benito, Philippe Isope, Matilde Cordero-Erausquin, Bernard Poulain, and members of the lab for their constructive comments throughout the project.

References

Abraham NM, Egger V, Shimshek DR, Renden R, Fukunaga I, Sprengel R, Seeburg PH, Klugmann M, Margrie TW, Schaefer AT, Kuner T (2010) Synaptic inhibition in the olfactory bulb accelerates odor discrimination in mice. Neuron 65:399-411.

671 Arenkiel BR, Peca J, Davison IG, Feliciano C, Deisseroth K, Augustine GJ, Ehlers MD, Feng G (2007) In
672 vivo light-induced activation of neural circuitry in transgenic mice expressing
673 channelrhodopsin-2. Neuron 54:205-218.
674 Aungst JL, Heyward PM, Puche AC, Karnup SV, Hayar A, Szabo G, Shipley MT (2003) Centre-surround
675 inhibition among olfactory bulb glomeruli. Nature 426:623-629.
676 Bardy C, Alonso M, Bouthour W, Lledo PM (2010) How, when, and where new inhibitory neurons
677 release neurotransmitters in the adult olfactory bulb. J Neurosci 30:17023-17034.
678 Boyd AM, Sturgill JF, Poo C, Isaacson JS (2012) Cortical feedback control of olfactory bulb circuits.
679 Neuron 76:1161-1174.
680 Boyd AM, Kato HK, Komiyama T, Isaacson JS (2015) Broadcasting of cortical activity to the olfactory
681 bulb. Cell Rep 10:1032-1039.
682 Burton SD, LaRocca G, Liu A, Cheetham CE, Urban NN (2017) Olfactory Bulb Deep Short-Axon Cells
683 Mediate Widespread Inhibition of Tufted Cell Apical Dendrites. J Neurosci 37:1117-1138.
684 Cang J, Isaacson JS (2003) In vivo whole-cell recording of odor-evoked synaptic transmission in the rat
685 olfactory bulb. J Neurosci 23:4108-4116.
686 Case DT, Burton SD, Gedeon JY, Williams SG, Urban NN, Seal RP (2017) Layer- and cell type-selective
687 co-transmission by a basal forebrain cholinergic projection to the olfactory bulb. Nat
688 Commun 8:652.
689 Castillo PE, Carleton A, Vincent JD, Lledo PM (1999) Multiple and opposing roles of cholinergic
690 transmission in the main olfactory bulb. J Neurosci 19:9180-9191.
691 Devore S, de Almeida L, Linster C (2014) Distinct roles of bulbar muscarinic and nicotinic receptors in
692 olfactory discrimination learning. J Neurosci 34:11244-11260.
693 Do JP, Xu M, Lee SH, Chang WC, Zhang S, Chung S, Yung TJ, Fan JL, Miyamichi K, Luo L, Dan Y (2016)
694 Cell type-specific long-range connections of basal forebrain circuit. Elife 5.
695 Economo MN, Hansen KR, Wachowiak M (2016) Control of Mitral/Tufted Cell Output by Selective
696 Inhibition among Olfactory Bulb Glomeruli. Neuron 91:397-411.
697 Eyre MD, Antal M, Nusser Z (2008) Distinct deep short-axon cell subtypes of the main olfactory bulb
698 provide novel intrabulbar and extrabulbar GABAergic connections. J Neurosci 28:8217-8229.
699 Fukunaga I, Berning M, Kollo M, Schmaltz A, Schaefer AT (2012) Two distinct channels of olfactory
700 bulb output. Neuron 75:320-329.
701 Fukunaga I, Herb JT, Kollo M, Boyden ES, Schaefer AT (2014) Independent control of gamma and
702 theta activity by distinct interneuron networks in the olfactory bulb. Nat Neurosci 17:1208-
703 1216.
704 Geramita M, Urban NN (2017) Differences in Glomerular-Layer-Mediated Feedforward Inhibition
705 onto Mitral and Tufted Cells Lead to Distinct Modes of Intensity Coding. J Neurosci 37:1428-
706 1438.
707 Ghatpande AS, Gelperin A (2009) Presynaptic muscarinic receptors enhance glutamate release at the
708 mitral/tufted to granule cell dendrodendritic synapse in the rat main olfactory bulb. J
709 Neurophysiol 101:2052-2061.
710 Gracia-Llanes FJ, Crespo C, Blasco-Ibanez JM, Nacher J, Varea E, Rovira-Esteban L, Martinez-Guijarro
711 FJ (2010) GABAergic basal forebrain afferents innervate selectively GABAergic targets in the
712 main olfactory bulb. Neuroscience 170:913-922.
713 Gschwend O, Abraham NM, Lagier S, Begnaud F, Rodriguez I, Carleton A (2015) Neuronal pattern
714 separation in the olfactory bulb improves odor discrimination learning. Nat Neurosci
715 18:1474-1482.
716 Hamamoto M, Kiyokage E, Sohn J, Hioki H, Harada T, Toida K (2017) Structural basis for cholinergic
717 regulation of neural circuits in the mouse olfactory bulb. J Comp Neurol 525:574-591.
718 Hangya B, Ranade SP, Lorenc M, Kepecs A (2015) Central Cholinergic Neurons Are Rapidly Recruited
719 by Reinforcement Feedback. Cell 162:1155-1168.
720 Isaacson JS, Strowbridge BW (1998) Olfactory reciprocal synapses: dendritic signaling in the CNS.
721 Neuron 20:749-761.

Kiyokage E, Pan YZ, Shao Z, Kobayashi K, Szabo G, Yanagawa Y, Obata K, Okano H, Toida K, Puche AC, Shipley MT (2010) Molecular identity of periglomerular and short axon cells. J Neurosci 30:1185-1196.

Kosaka K, Kosaka T (2007) Chemical properties of type 1 and type 2 periglomerular cells in the mouse olfactory bulb are different from those in the rat olfactory bulb. Brain Res 1167:42-55.

Kosaka T, Kosaka K (2008) Tyrosine hydroxylase-positive GABAergic juxtaglomerular neurons are the main source of the interglomerular connections in the mouse main olfactory bulb. Neurosci Res 60:349-354.

Kosaka T, Kosaka K (2011) "Interneurons" in the olfactory bulb revisited. Neurosci Res 69:93-99.

Lepousez G, Lledo PM (2013) Odor discrimination requires proper olfactory fast oscillations in awake mice. Neuron 80:1010-1024.

Linster C, Hasselmo ME (2000) Neural activity in the horizontal limb of the diagonal band of broca can be modulated by electrical stimulation of the olfactory bulb and cortex in rats. Neurosci Lett 282:157-160.

Liu S, Plachez C, Shao Z, Puche A, Shipley MT (2013) Olfactory bulb short axon cell release of GABA and dopamine produces a temporally biphasic inhibition-excitation response in external tufted cells. J Neurosci 33:2916-2926.

Liu S, Shao Z, Puche A, Wachowiak M, Rothermel M, Shipley MT (2015) Muscarinic receptors modulate dendrodendritic inhibitory synapses to sculpt glomerular output. J Neurosci 35:5680-5692.

Ma M, Luo M (2012) Optogenetic activation of basal forebrain cholinergic neurons modulates neuronal excitability and sensory responses in the main olfactory bulb. J Neurosci 32:10105-10116.

Macrides F, Davis BJ, Youngs WM, Nadi NS, Margolis FL (1981) Cholinergic and catecholaminergic afferents to the olfactory bulb in the hamster: a neuroanatomical, biochemical, and histochemical investigation. J Comp Neurol 203:495-514.

Markopoulos F, Rokni D, Gire DH, Murthy VN (2012) Functional properties of cortical feedback projections to the olfactory bulb. Neuron 76:1175-1188.

Metzger F, Repunte-Canonigo V, Matsushita S, Akemann W, Diez-Garcia J, Ho CS, Iwasato T, Grandes P, Itohara S, Joho RH, Knopfel T (2002) Transgenic mice expressing a pH and Cl- sensing yellow-fluorescent protein under the control of a potassium channel promoter. Eur J Neurosci 15:40-50.

Monory K et al. (2006) The endocannabinoid system controls key epileptogenic circuits in the hippocampus. Neuron 51:455-466.

Murphy GJ, Darcy DP, Isaacson JS (2005) Intraglomerular inhibition: signaling mechanisms of an olfactory microcircuit. Nat Neurosci 8:354-364.

Najac M, Sanz Diez A, Kumar A, Benito N, Charpak S, De Saint Jan D (2015) Intraglomerular lateral inhibition promotes spike timing variability in principal neurons of the olfactory bulb. J Neurosci 35:4319-4331.

Niedworok CJ, Schwarz I, Ledderose J, Giese G, Conzelmann KK, Schwarz MK (2012) Charting monosynaptic connectivity maps by two-color light-sheet fluorescence microscopy. Cell Rep 2:1375-1386.

Nunez-Parra A, Maurer RK, Krahe K, Smith RS, Araneda RC (2013) Disruption of centrifugal inhibition to olfactory bulb granule cells impairs olfactory discrimination. Proc Natl Acad Sci U S A 110:14777-14782.

Otazu GH, Chae H, Davis MB, Albeanu DF (2015) Cortical Feedback Decorrelates Olfactory Bulb Output in Awake Mice. Neuron 86:1461-1477.

Panzanelli P, Fritschy JM, Yanagawa Y, Obata K, Sassoe-Pognetto M (2007) GABAergic phenotype of periglomerular cells in the rodent olfactory bulb. J Comp Neurol 502:990-1002.

Paolini AG, McKenzie JS (1997) Intracellular recording of magnocellular preoptic neuron responses to olfactory brain. Neuroscience 78:229-242.

773 Parrish-Aungst S, Shipley MT, Erdelyi F, Szabo G, Puche AC (2007) Quantitative analysis of neuronal
774 diversity in the mouse olfactory bulb. J Comp Neurol 501:825-836.
775 Parsa PV, D'Souza RD, Vijayaraghavan S (2015) Signaling between periglomerular cells reveals a
776 bimodal role for GABA in modulating glomerular microcircuitry in the olfactory bulb. Proc
777 Natl Acad Sci U S A 112:9478-9483.
778 Rothermel M, Carey RM, Puche A, Shipley MT, Wachowiak M (2014) Cholinergic inputs from Basal
779 forebrain add an excitatory bias to odor coding in the olfactory bulb. J Neurosci 34:4654-
780 4664.
781 Salcedo E, Tran T, Ly X, Lopez R, Barbica C, Restrepo D, Vijayaraghavan S (2011) Activity-dependent
782 changes in cholinergic innervation of the mouse olfactory bulb. PLoS One 6:e25441.
783 Saunders A, Granger AJ, Sabatini BL (2015) Corelease of acetylcholine and GABA from cholinergic
784 forebrain neurons. Elife 4.
785 Schoppa NE, Kinzie JM, Sahara Y, Segerson TP, Westbrook GL (1998) Dendrodendritic inhibition in the
786 olfactory bulb is driven by NMDA receptors. J Neurosci 18:6790-6802.
787 Shao Z, Puche AC, Shipley MT (2013) Intraglomerular inhibition maintains mitral cell response
788 contrast across input frequencies. J Neurophysiol 110:2185-2191.
789 Shao Z, Puche AC, Liu S, Shipley MT (2012) Intraglomerular inhibition shapes the strength and
790 temporal structure of glomerular output. J Neurophysiol 108:782-793.
791 Shao Z, Puche AC, Kiyokage E, Szabo G, Shipley MT (2009) Two GABAergic intraglomerular circuits
792 differentially regulate tonic and phasic presynaptic inhibition of olfactory nerve terminals. J
793 Neurophysiol 101:1988-2001.
794 Smith RS, Hu R, DeSouza A, Eberly CL, Krahe K, Chan W, Araneda RC (2015) Differential Muscarinic
795 Modulation in the Olfactory Bulb. J Neurosci 35:10773-10785.
796 Smith TC, Jahr CE (2002) Self-inhibition of olfactory bulb neurons. Nat Neurosci 5:760-766.
797 Whitesell JD, Sorensen KA, Jarvie BC, Hentges ST, Schoppa NE (2013) Interglomerular lateral
798 inhibition targeted on external tufted cells in the olfactory bulb. J Neurosci 33:1552-1563.
799 Whitman MC, Greer CA (2007) Adult-generated neurons exhibit diverse developmental fates. Dev
800 Neurobiol 67:1079-1093.
801 Yokoi M, Mori K, Nakanishi S (1995) Refinement of odor molecule tuning by dendrodendritic synaptic
802 inhibition in the olfactory bulb. Proc Natl Acad Sci U S A 92:3371-3375.
803 Zaborszky L, Carlsen J, Brashear HR, Heimer L (1986) Cholinergic and GABAergic afferents to the
804 olfactory bulb in the rat with special emphasis on the projection neurons in the nucleus of
805 the horizontal limb of the diagonal band. J Comp Neurol 243:488-509.
806
807

Supplementary Figures

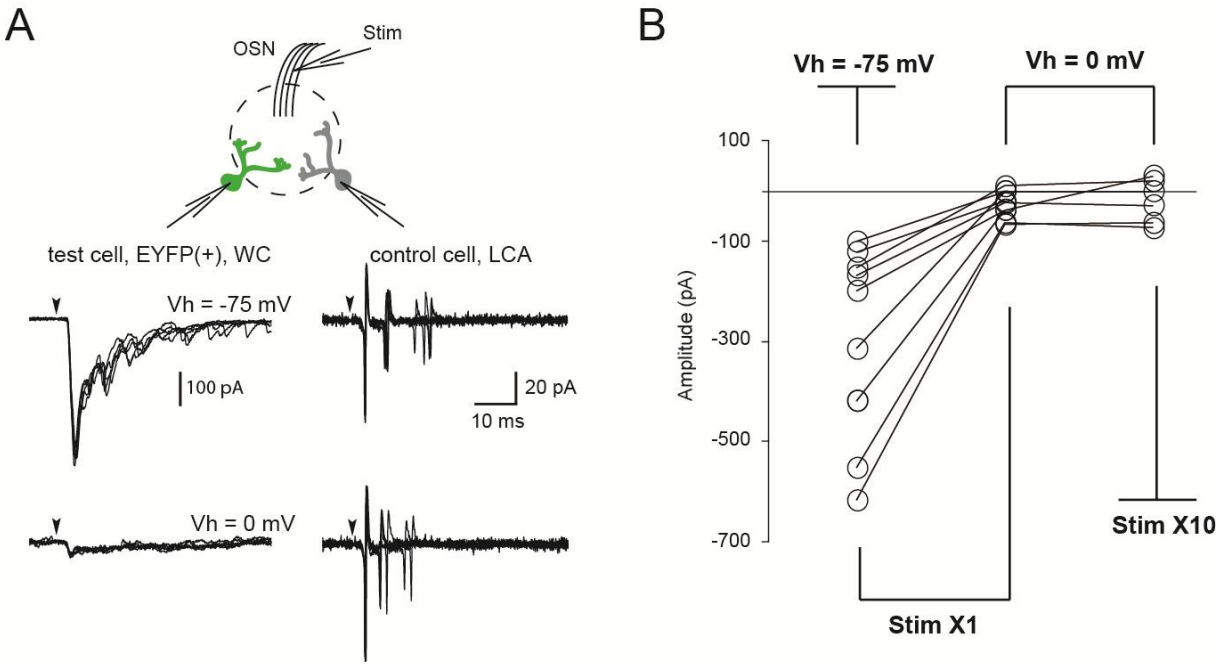

Supplementary Figure 1 : OSN-evoked firing of PG cells does not produce IPSCs in EYFP(+) PG cells. **A,** Paired recording of two PG cells projecting in the same glomerulus. The "test" EYFP(+) PG cell was recorded in the whole-cell configuration at Vh= -75 mV to monitor EPSCs (top) and at Vh= 0 mV to monitor IPSCs (bottom). The second "control" PG cell was recorded in the loose cell-attached configuration to monitor its firing. OSNs were stimulated at an intensity inducing the firing of the control PG cell (stim X1). **B,** The summary graph shows that OSN stimulations did not evoke any outward IPSC in the test cell even when the stimulation was increased by a factor of 10. Control cells were either EYFP(+) (n=4) or EYFP(-) (n=5).

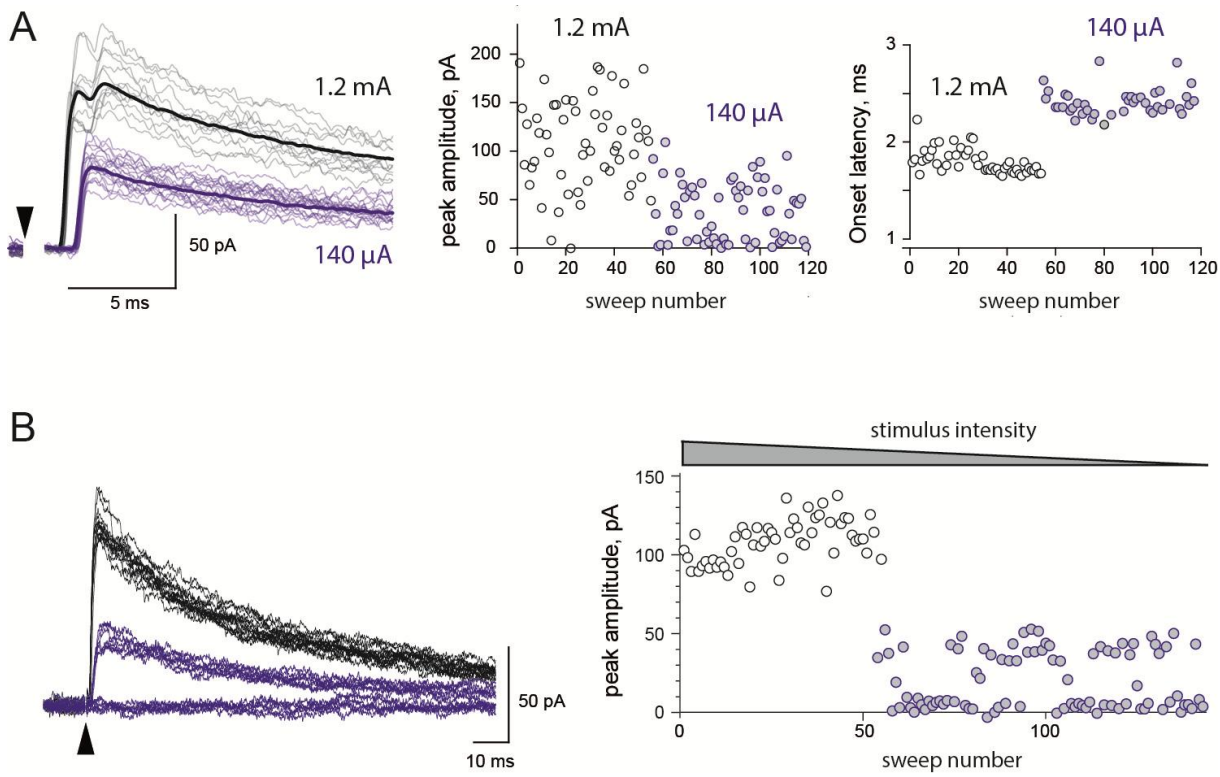

Supplementary Figure 2 : Multiple convergent inhibitory inputs of EYFP(+) PG cells can be recruited in the glomerular layer. A, Example of a EYFP(+) PG cells in which electrical stimulations in the glomerular layer at an intensity of 1.2 mA induced a short latency IPSC with two peaks (grey traces, average in black). Decreasing the intensity of stimulation to 140 µA evoked responses lacking the first peak and with longer latencies. Plots show the peak amplitudes (middle) and onset latencies (right) of consecutive episodes at the two intensities of stimulation. **B,** Example of another EYFP(+) PG cells in which progressive decrease of the stimulus strength suddenly reduced the amplitude of the response in a step-wise manner. Low intensity stimulations evoked an all-or-none minimal IPSC (blue traces).

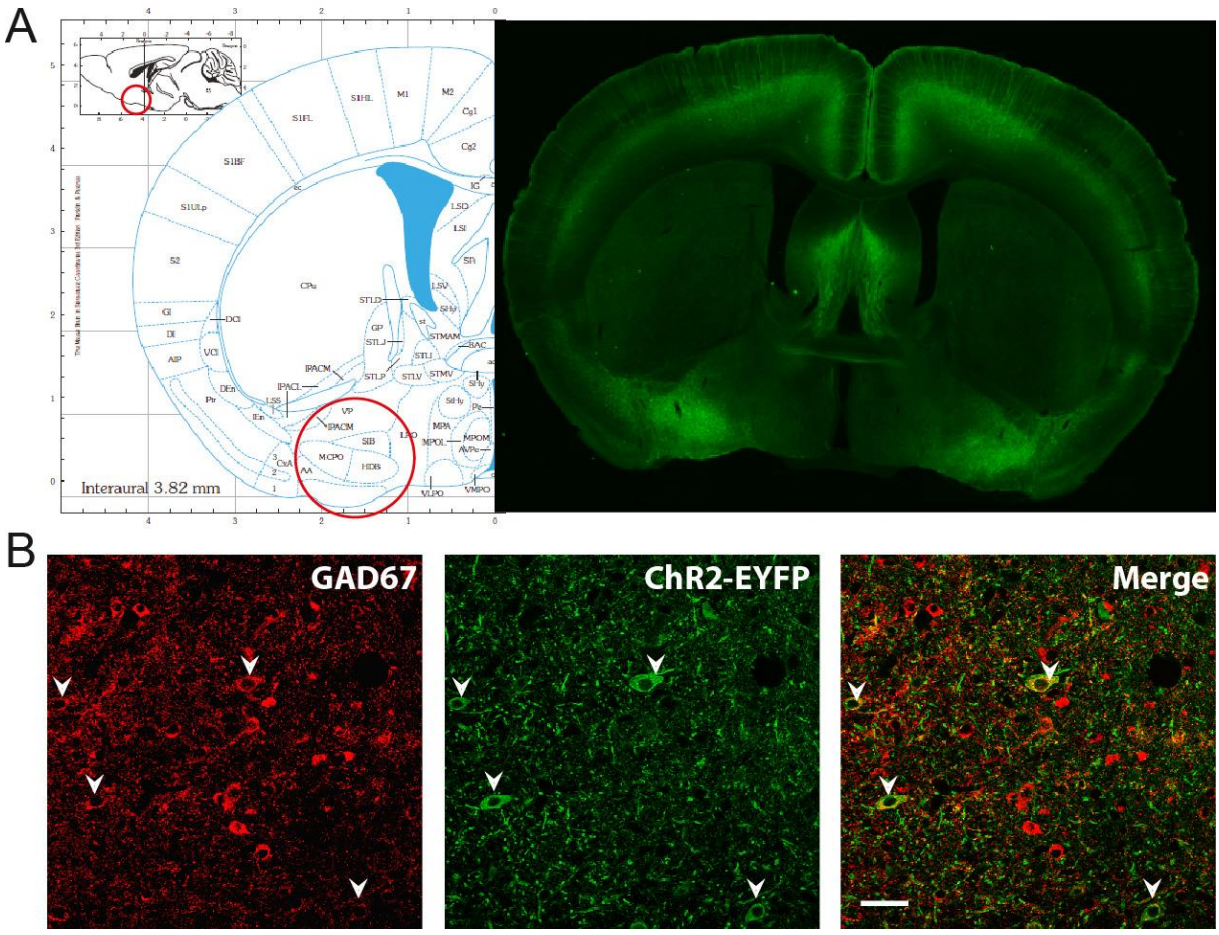

Supplementary Figure 3: Basal forebrain GABAergic neurons express ChR2-EYFP in the Thy1-ChR2-EYFP mouse. A, Coronal section from the brain of a Thy1-ChR2-EYFP mouse superimposed on the corresponding coronal section of the mouse brain (Franklin and Paxinos atlas) at 0.32 mm rostral from bregma. The HDB is located in the red circle. **B,** Immunofluorescence staining for GAD67 (red) and ChR2-EYFP in the HDB of a Thy1-ChR2-EYFP mouse. A fraction of the GABAergic neurons expresses ChR2 (white arrows). Scale bar 50 µm.